

## Solitary Waves on Vortex Lines in Ginzburg-Landau Models for the Example of Bose-Einstein Condensates

Natalia G. Berloff

*Department of Applied Mathematics and Theoretical Physics, University of Cambridge,  
Wilberforce Road, Cambridge, United Kingdom CB3 0WA*

(Received 28 June 2004; published 7 January 2005)

Axisymmetric disturbances that preserve their form as they move along the vortex lines in uniform Bose-Einstein condensates are obtained numerically by the solution of the Gross-Pitaevskii equation. A continuous family of such solitary waves is shown in the momentum ( $p$ )-substitution energy ( $\hat{\mathcal{E}}$ ) plane with  $p \rightarrow 0.09\rho\kappa^3/c^2$ ,  $\hat{\mathcal{E}} \rightarrow 0.091\rho\kappa^3/c$  as  $U \rightarrow c$ , where  $\rho$  is the density,  $c$  is the speed of sound,  $\kappa$  is the quantum of circulation, and  $U$  is the solitary wave velocity. It is shown that collapse of a bubble captured by a vortex line leads to the generation of such solitary waves in condensates. The various stages of collapse are elucidated. In particular, it is shown that during collapse the vortex core becomes significantly compressed, and after collapse two solitary wave trains moving in opposite directions are formed on the vortex line.

DOI: 10.1103/PhysRevLett.94.010403

PACS numbers: 03.75.Lm, 05.45.-a, 67.40.Vs, 67.57.De

An important role in the dynamics of nonlinear systems is played by solitary waves—the localized disturbances of the uniform field that are form preserving and move with a constant velocity. They appear in diverse contexts of science and engineering, such as fluid dynamics, transport along macromolecules, and fiber optic communications just to name a few. Considerable interest is attached to determining the entire sequence of solitary waves as they define possible states that can be excited in the system. Understanding the production, motion, and interactions of such solitary waves is one of the most significant questions in nonlinear science. In condensed matter systems solitary waves are topological objects since they owe their existence and perseverance to the topology of the order parameter field describing a medium with a broken symmetry. In this Letter I establish and study the production of a new class of solitary waves, each of which moves along vortex lines/topological defects in conservative Ginzburg-Landau systems. The discussion is restricted to a condensed matter system such as atomic Bose-Einstein condensates (BEC) where the evolution equation is the Gross-Pitaevskii (GP) model [1]; see Eq. (1) below (also known as the defocusing nonlinear Schrödinger equation in nonlinear optics). The applications are not restricted to the condensed matter systems due to the generality of the Ginzburg-Landau systems with implications to the motion of excitations along cosmic strings in the early Universe [2] and along topological defects in other ordered media: liquid crystals [3], nonequilibrium patterns, etc. Finally, the new solutions to the nonlinear Schrödinger equation which this Letter presents are of interest when so few have been derived in multidimensions.

Symmetry-breaking transitions in equilibrium systems can be described by an energy functional,  $\mathcal{E} = \int \mathcal{L}dV$ , in terms of a Lagrangian  $\mathcal{L}$ . The simplest form of the Lagrangian, capable of describing the

quenching beyond the critical point where the disordered state becomes unstable and the symmetry is spontaneously broken, is a Ginzburg-Landau Lagrangian  $\mathcal{L} = \frac{1}{2} \times [|\nabla\psi|^2 + \frac{1}{2}(1 - |\psi|^2)^2]$  dependent on a complex scalar order parameter  $\psi$ . The evolution equation describing the relaxation to the equilibrium state in an energy-preserving (conservative) system is given by the Euler-Lagrange equation  $\psi_t = -i\partial\mathcal{E}/\partial\psi^*$  that we write as

$$-2i\frac{\partial\psi}{\partial t} = \nabla^2\psi + (1 - |\psi|^2)\psi. \quad (1)$$

A phase singularity of a complex field  $\psi$  given by  $\psi = 0$  is called a quantized vortex or topological defect depending on a particular application. The total change of phase around any closed contour must be a multiple of  $2\pi$  and only quantized vortices with the total change of phase  $2\pi$  are topologically stable.

Such a general reasoning gives a simple explanation why Eq. (1) has a universal meaning and has been applied to a variety of systems [4]. In particular, it described accurately both equilibrium and dynamical properties of BEC [5]. The GP model has been remarkably successful in predicting the condensate shape in an external potential, the dynamics of the expanding condensate cloud, and the motion of quantized vortices; it is also a popular qualitative model of superfluid helium. For these systems Eq. (1) is written in dimensionless variables such that the unit of length corresponds to the healing length  $\xi$ , the speed of sound  $c = 1/\sqrt{2}$ , and the density at infinity  $\rho_\infty = |\psi_\infty|^2 = 1$ .

The straight line vortex positioned along the  $z$  axis in the absence of any other solitary waves is obtained by rewriting (1) in cylindrical coordinates  $(s, \theta, z)$  and using the ansatz  $\psi_0 = R(s)\exp(i\theta)$ . The resulting solution for  $R(s)$  was found numerically in the first reference of [1] and approximated in [6]. The infinitesimal perturbations of a rectilinear vortex in the GP model may be bound or

free, depending on their angular and axial wave numbers,  $m$  and  $k$ . The free waves radiate energy acoustically to infinity, while the bound states do not. The low frequency modes  $m = 1$ , which displace the axis of the vortex, are found to be bound for all  $k$  [7,8]. The low frequency modes  $m = 2$  are also bound when  $k$  is sufficiently large, but are free for small  $k$  [8].

A family of fully three-dimensional solitary waves was found by Jones and Roberts (JR) [9] who integrated Eq. (1) numerically and determined the entire sequence of solitary wave solutions of the GP equation, such as vortex rings and finite amplitude sound waves named rarefaction pulses. They showed the location of the sequence on the momentum,  $p$ , energy,  $\mathcal{E}$ , plane, that I refer to as the JR dispersion curve. In three dimensions they found two branches meeting at a cusp where  $p$  and  $\mathcal{E}$  assume their minimum values,  $p_m$  and  $\mathcal{E}_m$ . As  $p \rightarrow \infty$  on each branch,  $\mathcal{E} \rightarrow \infty$ . On the lower branch the solutions are asymptotic to large vortex rings. As  $\mathcal{E}$  and  $p$  decrease from infinity along the lower branch, the solutions begin to lose their similarity to large vortex rings. Eventually, for a momentum  $p_0$  slightly greater than  $p_m$ , they lose their vorticity ( $\psi$  loses its zero), and thereafter the solitary solutions may better be described as ‘‘rarefaction waves.’’ The upper branch consists entirely of these and, as  $p \rightarrow \infty$  on this branch, the solutions approach asymptotically the rational soliton solution of the Kadomtsev-Petviashvili type I equation.

In what follows I determine the entire family of axisymmetric ( $m = 0$ ) solitary wave solutions that move along the straight line vortex and relate them to the JR dispersion curve. In Eq. (1) written in cylindrical coordinates  $(s, \theta, z)$  I take the ansatz  $\psi = [R(s) + \phi(s, z)] \times \exp(i\theta)$  and assume that the disturbance  $\phi(s, z)$  moves with velocity  $U$  in the positive  $z$  direction. In the frame of reference moving with the solitary wave,  $\phi(s, z)$  satisfies

$$2iU \frac{\partial \phi}{\partial z} = \frac{1}{s} \frac{\partial}{\partial s} \left[ s \frac{\partial \phi}{\partial s} \right] + \frac{\partial^2 \phi}{\partial z^2} - \frac{\phi}{s^2} + [1 - 2R^2 - R(\phi + 2\phi^*) - |\phi|^2] \phi - R^2 \phi^*. \quad (2)$$

The disturbance is localized, so the boundary condition is  $\phi(s, z) \rightarrow 0$ , as  $|\mathbf{x}| \rightarrow \infty$  in all directions of  $\mathbf{x}$ . In view of the asymptotic expansions at infinity [9], I introduce stretched variables  $z' = z$  and  $s' = s\sqrt{1 - 2U^2}$  and map the infinite domain onto the box  $(0, \frac{\pi}{2}) \times (-\frac{\pi}{2}, \frac{\pi}{2})$  using the transformation  $\hat{z} = \tan^{-1}(Lz')$  and  $\hat{s} = \tan^{-1}(Ls')$ , where  $L$  is a constant  $\sim 0.1-0.4$ . Transformed Eq. (2) was expressed in second-order finite difference form using  $250 \times 200$  grid points, and the resulting nonlinear equations were solved by the Newton-Raphson iteration procedure using banded matrix linear solver based on the biconjugate gradient stabilized iterative method with preconditioning. For each solitary wave two quantities were calculated: the nonzero ( $z$ ) component of the momentum [9]

$$p = \frac{1}{2i} \int [\nabla \psi (\psi^* - 1) - \nabla \psi^* (\psi - 1)] dV \quad (3)$$

and the substitution energy,  $\hat{\mathcal{E}}$ , which is the difference between the energy of the vortex-solitary wave complex and the energy of the vortex line,

$$\hat{\mathcal{E}} = \frac{1}{2} \int |\nabla \psi|^2 - |\nabla \psi_0|^2 + \frac{1}{2} (1 - |\psi|^2)^2 - \frac{1}{2} (1 - |\psi_0|^2)^2 dV. \quad (4)$$

By performing the variation  $\psi \rightarrow \psi + \delta\psi$  in (3) and (4) and discarding surface integrals that vanish provided  $\delta\psi \rightarrow 0$  for  $\mathbf{x} \rightarrow \infty$ , we see that  $U = \partial \hat{\mathcal{E}} / \partial p$ , where the derivative is taken along the solitary wave sequence. The same expression is obeyed by the sequences of classical vortex rings in an incompressible fluid and by the solitary waves of [9]. I also note that if we multiply Eq. (2) by  $z \partial \psi^* / \partial z$  and integrate by parts we get  $\hat{\mathcal{E}} = \int |\partial \psi / \partial z|^2 dV$ , similarly to the expression for the energy of the JR solitons [10]. This expression was used as a check of the numerical accuracy. As  $p \rightarrow \infty$ ,  $\hat{\mathcal{E}} \rightarrow \infty$  and the solitary wave solutions are represented by large vortex rings moving along the vortex line. As  $\hat{\mathcal{E}}$  and  $p$  decrease from infinity, the radii of the rings decrease and for a momentum  $p_0 \approx 78$ ,  $\phi(s, z) = 0$  on the  $z$  axis only. To distinguish these solutions from vortex rings and to emphasize the analogy with the JR solitary waves, these solutions are called rarefaction waves as well. Table I shows the velocity, substitution energy, momentum, and radius of the solitary wave solutions found. Figure 1 shows the momentum-energy curve of the solutions in comparison with the JR dispersion curve. Notice that unlike the JR dispersion curve, there is no cusp on the energy-momentum plane. As  $U \rightarrow c$  neither  $\hat{\mathcal{E}}$  nor  $p$  goes to infinity; instead  $\hat{\mathcal{E}} \rightarrow 32$  and  $p \rightarrow 45$  which lies below the JR cusp. It was suggested in [9,10] that every solitary wave on the upper branch is unstable, since it is energetically favorable for it to ‘‘collapse’’ onto the lower branch of smaller energy at the same momentum. Since the rarefaction solitary waves on the vortex line do not have any other solitary states of lower energy at the

TABLE I. The velocity,  $U$ , substitution energy,  $\hat{\mathcal{E}}$ , momentum,  $p$ , and radius,  $b$ , of the solitary wave solutions moving along the straight line vortex.

$U$	0.4	0.45	0.5	0.55	0.6	0.61
$\hat{\mathcal{E}}$	142	113	90.7	72.4	56.9	54.0
$p$	262	193	145	110	83.2	78.4
$b$	4.18	3.62	3.08	2.41	1.05	0.1
$U$	0.63	0.65	0.67	0.69	0.7	0.705
$\hat{\mathcal{E}}$	48.4	43.0	37.8	33.3	32.2	32.1
$p$	69.4	61.0	53.1	46.5	45.0	45.0

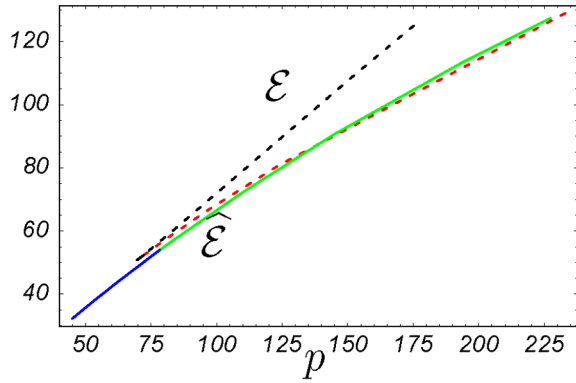


FIG. 1 (color online). The dispersion curves for two families of the axisymmetric solitary wave solutions. The dashed line represents the JR dispersion curve. The part of the curve that corresponds to the vortex rings is shown in gray (red). The solid line gives the substitution energy as a function of momentum for the solitary waves moving along the vortex line with vortex rings shown in light gray (green).

same momentum, this may suggest that they are stable. The substitution energy,  $\hat{E}$ , and momentum,  $p$ , of our vortex rings are larger than corresponding values of  $E$  and  $p$  of the JR rings moving with the same velocity. If the vortex rings of the same radii are compared, our rings have lower energy and momentum. Figure 2 shows the density isoplots and the density contour plots of two

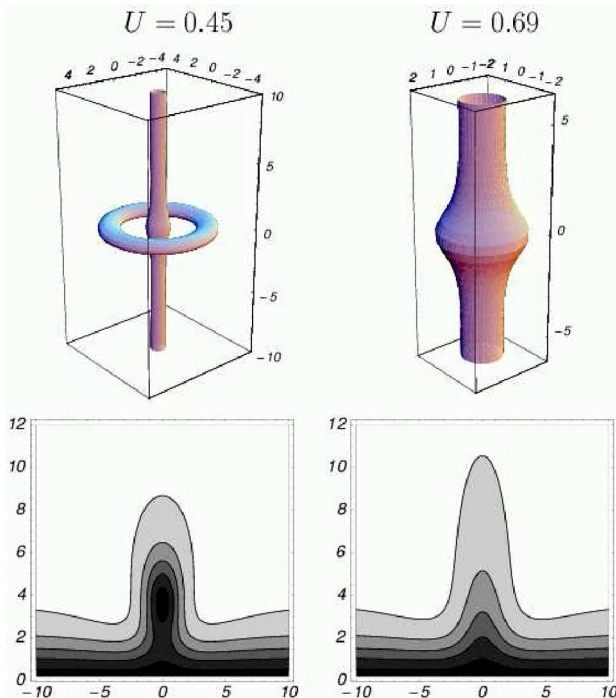


FIG. 2 (color online). Two solitary wave solutions moving with velocity  $U = 0.45$  (left) and  $U = 0.69$  (right) along the straight line vortex. The density isoplots at  $\rho = 0.1$  (left) and  $\rho = 0.3$  (right) are shown in the two top panels. The density contour plots (0.1, 0.3, 0.5, 0.7, 0.9) at the cross section  $\theta = 0$  are shown in the two bottom panels.

representative solutions such as a rarefaction pulse and a vortex ring. Notice the vortex core expansion at the center of the vortex ring due to a decrease in pressure in the high velocity region.

A question that arises after new solutions are found theoretically is how to create them in an actual physical system. In [11] we established a new mechanism of vortex nucleation by collapsing bubbles in the context of the GP model. These results referred to the collapse of cavitated bubbles generated by ultrasound in the megahertz frequency range that have been observed to produce quantized vortices in superfluid helium [12]. Also, vortices form as a result of bubbles colliding during a first-order phase transition of an early Universe [2]. In [13] we have shown that a soft bubble, carved out in the surrounding fluid by an electron through its zero-point motion, becomes trapped in vortex lines. The Bernoulli effect of the flow created by the flow circulation around the vortex propels the bubble and vortex towards one another with a force approximately proportional to  $s^{-3}$ , where  $s$  is the closest distance between them. As the bubble becomes trapped in the vortex core, the flow round the bubble acquires circulation that it previously could not possess. After the emission of Kelvin waves, which were excited on the vortex core during the capture, the bubble-vortex complex stabilizes to an axisymmetric form depicted in

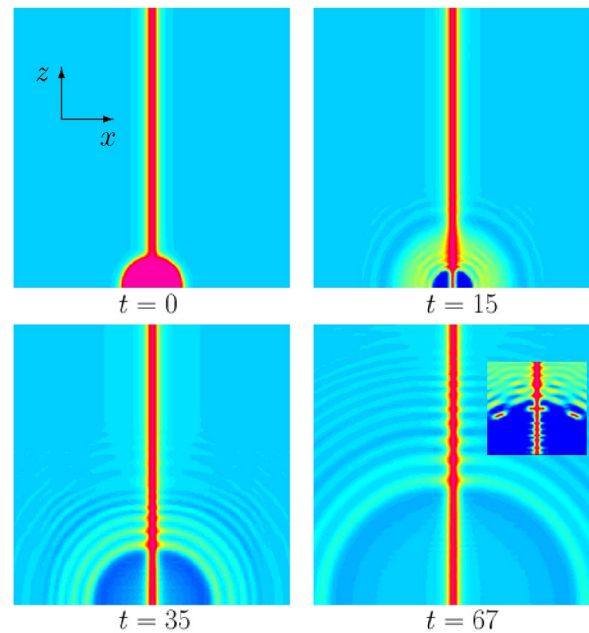


FIG. 3 (color online). Collapse of the bubble of radius  $a = 10$  trapped by the vortex line. The density plots of the cross section of the solution of Eq. (1) with initial state (5) at  $y = 0$ ,  $x \in [-50, 50]$ ,  $z \in [0, 100]$  are shown. The inset shows a vortex ring traveling along the  $z$  axis generated after the collapse of the bubble of radius  $a = 50$  at  $t = 100$ . Two vortex rings of smaller radii are also seen to the left and to the right. Both low and high density regions are shown in darker shades to emphasize intermediate density regions.

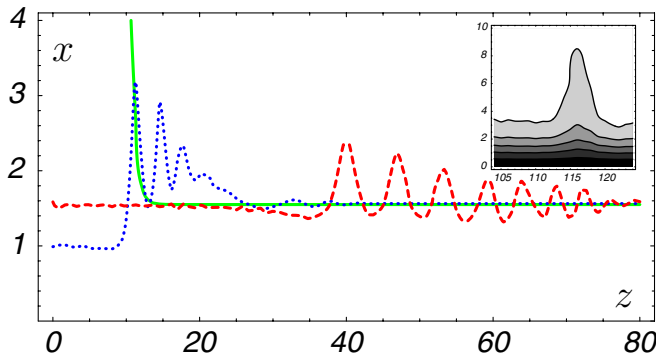


FIG. 4 (color online). Collapse of the bubble of radius  $a = 10$ . The contour  $\rho/\rho_\infty = 4/5$  is shown at  $t = 0$  (solid green line),  $t = 20$  (dotted blue line), and  $t = 60$  (dashed red line). The density contour plot of the condensate showing a well-separated solitary wave at  $t = 166$  is given in the inset (compare this with the bottom right panel of Fig. 2).

Fig. 2 of [13]; see also Fig. 3 ( $t = 0$ ) below. One could expect that a similar capture of bubbles created by ultrasound takes place in BEC and that vacuum bubbles get trapped in cosmic strings. The captured bubble will then collapse sending axisymmetric waves along the vortex line. To elucidate the stages of this collapse I performed the numerical simulations of the GP equation (1) starting with the initial condition

$$\psi(\mathbf{x}, t = 0) = \begin{cases} R(s)e^{i\theta}\tanh\left(\frac{r-a}{\sqrt{2}}\right) & \text{if } r > a, \\ 0 & \text{if } 0 \leq r \leq a, \end{cases} \quad (5)$$

where  $r^2 = x^2 + y^2 + z^2$ . The initial state (5) gives an accurate representation of the stationary complex, which consists of the straight line vortex on the  $z$  axis and the bubble of radius  $a$  centered at the origin. The surface of the bubble is assumed to be an infinite potential barrier to the condensate particles, so no bosons can be found inside the bubble ( $\psi = 0$ ) before the collapse, and this is why  $\tanh(\ell/\sqrt{2})$ , which is the wave function of the condensate distance  $\ell$  away from a solid wall, is relevant here. “Softer” bubbles that allow some condensate penetration were also considered by reducing the slope of the hyperbolic tangent, but no significant difference was detected. I performed fully three-dimensional calculations for cavities of various radii in a computational cube with sides of 200 healing lengths [14]. Figure 3 shows the density plots of the portion of the cross section at  $y = 0$  at various times after the collapse of a bubble of radius  $a = 10$ . Figure 4 depicts density contours  $\rho/\rho_\infty = 4/5$  at times  $t = 0, 20$ , and  $60$ . The time-dependent evolution of the condensate during and after the bubble’s collapse involves several stages. During the first stage dispersive and nonlinear wave trains are generated at the surface of the bubble. This stage of the evolution is characterized by a flux of particles towards the center of the cavity. This

creates an inward force acting on the vortex core reducing the cross-sectional area of the core. The reduction by a factor of 1.5 is seen on the  $t = 15$  snapshot of Fig. 3 and on the density contour of Fig. 4 at  $t = 20$ . The next stage in the evolution is outward expansion of the condensate that overfilled the cavity. The instability mechanism for collapsing bubbles in the absence of the straight line vortex, which we described in detail in [11], sets in, leading to the production of vortex rings and rarefaction pulses mostly along the vortex line, as the energy and momentum necessary for their creation is lower there. As the train of solitary waves starts moving away from the collapsed bubble (see Figs. 3 and 4), the distance between them increases since they move with different velocities. In time each individual solitary wave approaches its localized form found in the first part of this Letter; see the inset of Fig. 4. During collapse of a bubble of a larger radius ( $a \geq 28$ ) vortex rings are generated together with rarefaction pulses on the vortex line; see the inset of Fig. 3.

The author is grateful to Professor Paul Roberts and Professor Boris Svistunov for useful comments about this manuscript. The support from NSF Grant No. DMS-0104288 is acknowledged.

- 
- [1] V. L. Ginzburg and L. P. Pitaevskii, *Sov. Phys. JETP* **34**, 1240 (1958); E. P. Gross, *Nuovo Cimento* **20**, 454 (1961).
  - [2] A. M. Srivastava, *Phys. Rev. D* **46**, 1353 (1992); G. E. Volovik, *Phys. Rep.* **351**, 195 (2001); K. Kasamatsu and M. Tsubota, *J. Low Temp. Phys.* **126**, 315 (2002).
  - [3] I. Chuang, N. Turok, and B. Yürke, *Phys. Rev. Lett.* **66**, 2472 (1991).
  - [4] L. M. Pismen, *Vortices in Nonlinear Fields: From Liquid Crystals to Superfluids: From Nonequilibrium Patterns To Cosmic Strings* (Clarendon Press, Oxford, 1999).
  - [5] A. L. Fetter and A. A. Svidzinsky, *J. Phys. Condens. Matter* **13**, R135 (2001).
  - [6] N. G. Berloff, *J. Phys. A* **37**, 1617 (2004).
  - [7] L. P. Pitaevskii, *Sov. Phys. JETP* **13**, 451 (1961).
  - [8] P. H. Roberts, *Proc. R. Soc. London A* **459**, 597 (2003).
  - [9] C. A. Jones and P. H. Roberts, *J. Phys. A* **15**, 2599 (1982).
  - [10] C. A. Jones, S. J. Putterman, and P. H. Roberts, *J. Phys. A* **19**, 2991 (1986).
  - [11] N. G. Berloff and C. F. Barenghi, *Phys. Rev. Lett.*, **93**, 090401 (2004).
  - [12] R. D. Finch, R. Kagiwada, M. Barmatz, and I. Rudnick, *Phys. Rev.* **134**, A1425 (1964); R. F. Carey, J. A. Rooney, and C. W. Smith, *Phys. Lett. A* **65**, 311 (1978).
  - [13] N. G. Berloff and P. H. Roberts, *Phys. Rev. B* **63**, 024510 (2000).
  - [14] I used the same numerical method as in Ref. [15]. The faces of the computational box were open to allow sound waves to escape.
  - [15] N. G. Berloff and P. H. Roberts, *J. Phys. A* **33**, 4025 (2000).